Mechanical Systems and Signal Processing 223 (2025) 111909

Contents lists available at ScienceDirect

Mechanical Systems and Signal Processing

journal homepage: www.elsevier.com/locate/ymssp

# Estimation of velocity response spectrum using acceleration response spectrum

Zheng Liu [a], Yan-Gang Zhao [a], Haizhong Zhang [b,*]

[a] Key Laboratory of Urban Security and Disaster Engineering of Ministry of Education, Beijing University of Technology, Beijing 100124, China
[b] Faculty of Agriculture,Yamagata University, 1-23, Wakaba-machi, Tsuruoka-shi, Yamagata 997-8555, Japan

A R T I C L E I N F O

*Keywords:*
Velocity response spectrum
Acceleration response spectrum
Pseudo-velocity response spectrum
Random vibration theory

A B S T R A C T

The velocity response spectrum (SV) plays an important role in the seismic design of structures that incorporate supplementary velocity-dependent dampers, which can be approximated by the pseudo-velocity response spectrum converted from the acceleration response spectrum (SA). However, the error of this approximation is significant for short and long periods. This paper aims to develop a model for transforming the SA into the SV. To systematically explore the relationship between SA and SV and find the parameters affecting it, a theoretical SA-SV relationship is derived based on random vibration theory. Accordingly, statistical analyses using a large number of ground motion records were conducted to establish a simple model for transforming the SA to the SV. The results of the proposed model are found to agree very well with those obtained from actual seismic motion records. This study promotes the accurate conversion from SA to SV and is particularly useful for the seismic design of structures equipped with velocity-dependent dampers.

## 1. Introduction

In the seismic design of structures that incorporate supplementary velocity-dependent dampers, it is essential to utilize the velocity response spectrum (SV) to compute the maximal relative velocity values across the ends of dampers and establish their corresponding design forces (FEMA-450) [1]. In addition, the SV is also crucial for seismic analysis of structures with nonproportional damping in the context of the complex mode response spectrum method [2,3]. However, many seismic codes, e.g., the Eurocode 8 [4] and ASCE/SEI7-10 [5], only provide the displacement response spectrum (SD) or pseudo acceleration response spectrum (PSA) as the seismic design load. The SV can be approximated using the pseudo-velocity response spectrum ($PSV_{SD}$) that is obtained from the SD using the well-known approximated relationship $PSV_{SD} = \omega SD$. However, the validity of this approximation has been noted to be limited to the intermediate-period range, and the error is significant for short and long periods. Therefore, many studies [6–15] have discussed the conversion formulas from SD (or PSA) to SV. For example, Liu *et al.* [15] proposed a conversion model from SD (or PSA) to SV, considering the effects of magnitude, distance, and site class, based on a large number of real ground motion records.

Different from Eurocode 8 and ASCE/SEI7-10, many seismic codes, such as the Chinese seismic code GB50011–2010 [16] and the Japanese Building Standard [17], only provide the acceleration response spectrum (SA) as the seismic design load. The SV can also be approximated using the pseudo-velocity response spectrum (PSV) that is obtained from the SA using the approximated relationship $SV \approx PSV = SA/\omega$. Similarly, the error of this approximation is found to be significant for short and long periods. In addition, Zhang

* Corresponding author.
*E-mail address:* zhang@tds1.tr.yamagata-u.ac.jp (H. Zhang).

https://doi.org/10.1016/j.ymssp.2024.111909
Received 30 March 2024; Received in revised form 5 August 2024; Accepted 1 September 2024

and Zhao [18] and Hang *et al.* [19] have demonstrated that SA is significantly different from PSA, particularly when the structural damping ratio is large and the structural period is long. Therefore, using the current conversion models of PSA (or SD) to SV developed previously [15] is also not feasible for converting SA to SV.

The objective of this paper is to establish a model that enables the conversion of the SA to the SV. The remainder of this article is structured in the following manner. In Section 2, a theoretical equation was proposed to connect SA and SV based on random vibration theory (RVT). Based on the derived theoretical equation, a systematic investigation and clarification of the relationship between SA and SV is conducted, in Section 3. In Section 4, a model was established to convert SA to SV based on regression analysis of a large number of ground motion records. In Section 5, the conclusions are given.

## 2. Theoretical equation connecting SA and SV

To obtain a conversion model from SA to SV, it is necessary to understand the relationship between the two spectra and find controlling parameters that need to be incorporated into the model. For this purpose, a theoretical approach between SA and SV explicitly including various structural and seismological parameters is desirable. Such an approach allows a systematic investigation of each single parameter's effects on the SA-SV relationship by constraining all other parameters. Moreover, a theoretical approach not only can analyze superficial phenomena but also provide a more in-depth analysis of influencing factors (as conducted in Section 3.2).

### 2.1. Theoretical derivation

In this section, a theoretical equation connecting SA and SV is derived based on RVT. The RVT method states that the peak value of a signal can be obtained by multiplying its root mean square (rms) value with an estimated peak factor. Under this principle, Boore [20] developed an equation to calculate the SD of earthquake ground motion, which is formulated as follows:

$$SD(\overline{\omega},\xi) = pf_{rd}\sqrt{\frac{1}{D_{\text{rms}}\pi}\int_0^\infty |Y(\omega)Hd(\omega,\overline{\omega},\xi)|^2 d\omega} \tag{1}$$

in which, $pf_{rd}$ and the square root part of Eq. (1) represent the peak factor and rms value of the displacement response of the single-degree-of-freedom (SDOF) oscillator, respectively; $\overline{\omega}$ and $\xi$ correspond to the circular frequency and damping ratio of the SDOF oscillator; $D_{\text{rms}}$ represent the rms duration for the oscillator response; $|Y(\omega)Hd(\omega,\overline{\omega},\xi)|$ represents the Fourier amplitude spectrum (FAS) of the oscillator displacement response, which is obtained by multiplying the FAS of the ground acceleration, $Y(\omega)$, with the oscillator transfer function for the relative displacement response, $|Hd(\omega,\overline{\omega},\xi)|$,

$$|Hd(\omega,\overline{\omega},\xi)| = \frac{1}{\sqrt{(2\xi\omega\overline{\omega})^2 + (\omega^2-\overline{\omega}^2)^2}} \tag{2}$$

in which, $\omega$ is the circular frequency of FAS. It is essential to distinguish between the oscillator circular frequency $\overline{\omega}$ and the circular frequency of FAS $\omega$.

To calculate the SD, it is necessary to ascertain the oscillator-response peak factor. Numerous models have been developed to determine peak factors for RVT analyses [21–23]. Despite the widespread utilization of the Cartwright and Longuet-Higgins [21] model in engineering seismology and site-response analyses [24], the Vanmarcke [23] model offers superior capabilities for estimating the peak factor [25]. According to the Vanmarcke [23] model, the cumulative distribution function (CDF) of the oscillator response peak factor, $pf_{rd}$, can be obtained by:

$$P(pf_{rd}<r) = \left[1-e^{(-r^2/2)}\right]\times\exp\left[-2f_z\exp(-r^2/2)D\frac{\left(1-e^{-\delta^{1.2}r\sqrt{\pi/2}}\right)}{(1-e^{r^2/2})}\right] \tag{3}$$

where, $D$ represents the duration of ground motion, which is different from $D_{\text{rms}}$ representing the rms duration for the oscillator response. $\delta$ denotes the bandwidth factor of the oscillator response FAS, it can be expressed as:

$$\delta = \sqrt{1-\frac{m_1^2}{m_0 m_2}} \tag{4}$$

in which, $m_0$, $m_1$, and $m_2$ represent the zeroth-, first-, and second-order moments of the oscillator response FAS correspondingly, and the $n$th-order spectral moment is defined as follows:

$$m_n = \frac{1}{\pi}\int_0^\infty \omega^n |Y(\omega)Hd(\omega,\overline{\omega},\xi)|^2 d\omega \tag{5}$$

$f_z$ appearing in Eq. (3) represents the rate of zero crossing, which is defined as follows:

$$f_z = \frac{1}{2\pi}\sqrt{\frac{m_2}{m_0}} \tag{6}$$

Based on the principles of RVT, it can be easily known that the SA is equivalent to the oscillator-response peak factor multiplied by the rms value of the oscillator acceleration response,

$$SA(\overline{\omega},\xi) = pf_{ra}\sqrt{\frac{1}{D_{\mathrm{rms}}\pi}\int_0^\infty |Y(\omega)Ha(\omega,\overline{\omega},\xi)|^2 d\omega} \tag{7}$$

in which, $pf_{ra}$ and the square root part of Eq. (7) represent the peak factor and rms value of the oscillator acceleration response, respectively; $|Y(\omega)Ha(\omega,\overline{\omega},\xi)|$ represents the FAS of the oscillator acceleration response, which is obtained by multiplying the FAS of the ground acceleration, $Y(\omega)$, with the oscillator transfer function for the absolute acceleration response, $|Ha(\omega,\overline{\omega},\xi)|$,

$$|Ha(\omega,\overline{\omega},\xi)| = \frac{\sqrt{(2\xi\omega/\overline{\omega})^2+1}}{\sqrt{(2\xi\omega/\overline{\omega})^2+\left[(\omega/\overline{\omega})^2-1\right]^2}} \tag{8}$$

Similarly, SV is equal to the rms value of the oscillator velocity response multiplied by the oscillator-response peak factor,

$$SV(\overline{\omega},\xi) = pf_{rv}\sqrt{\frac{1}{D_{\mathrm{rms}}\pi}\int_0^\infty |Y(\omega)Hv(\omega,\overline{\omega},\xi)|^2 d\omega} \tag{9}$$

in which, $pf_{rv}$ and the square root part of Eq. (9) represent the peak factor and rms value of the oscillator velocity response, respectively; $|Y(\omega)Hv(\omega,\overline{\omega},\xi)|$ represents the FAS of the oscillator velocity response, which is obtained by multiplying the FAS of the ground acceleration, $Y(\omega)$, with the oscillator transfer function for the relative velocity response, $|Hv(\omega,\overline{\omega},\xi)|$,

$$|Hv(\omega,\overline{\omega},\xi)| = \frac{\omega}{\sqrt{(2\xi\omega\overline{\omega})^2+(\omega^2-\overline{\omega}^2)^2}} \tag{10}$$

Then, the relationship between SA and SV can be expressed in the form of $SV/SA$, which can be obtained by dividing Eq. (9) by Eq. (7),

$$\frac{SV}{SA} = \sqrt{\frac{\int_0^\infty |Y(\omega)Hv(\omega,\overline{\omega},\xi)|^2 d\omega}{\int_0^\infty |Y(\omega)Ha(\omega,\overline{\omega},\xi)|^2 d\omega}} \times \frac{pf_{rv}}{pf_{ra}} \tag{11}$$

The oscillator-response peak factors for SA and SV can be obtained using Eq. (3) just by replacing the $|Y(\omega)Hd(\omega,\overline{\omega},\xi)|$ in Eq. (5) with $|Y(\omega)Ha(\omega,\overline{\omega},\xi)|$ and $|Y(\omega)Hv(\omega,\overline{\omega},\xi)|$, respectively. As to the rms duration $D_{\mathrm{rms}}$, only the equation for SD has been discussed previously [26], and those for SA and SV have never been discussed. In this study, for the sake of simplicity, it is assumed that the rms durations for SA and SV are the same as that for SD, which can be found reasonably in the following section. Therefore, the rms duration $D_{\mathrm{rms}}$ disappears in Eq. (11).

Since it is traditionally considered that SV and PSV are similar, this study discusses the relationship between SV and SA by investigating the ratio of SV to PSV, which is expressed as,

$$\frac{SV(\overline{\omega},\xi)}{PSV(\overline{\omega},\xi)} = \frac{SV}{SA/\omega} = \sqrt{\frac{\int_0^\infty |Y(\omega)Hv(\omega,\overline{\omega},\xi)|^2 d\omega}{\int_0^\infty |Y(\omega)Hpv(\omega,\overline{\omega},\xi)|^2 d\omega}} \times \frac{pf_{rv}}{pf_{ra}} \tag{12}$$

in which, $|Hpv(\omega,\overline{\omega},\xi)|$ is the absolute value of the oscillator transfer function for the PSV,

$$|Hpv(\omega,\overline{\omega},\xi)| = \frac{\sqrt{(2\xi\omega/\overline{\omega})^2+1}}{\sqrt{(2\xi\omega)^2+(\omega^2/\overline{\omega}-\overline{\omega})^2}} \tag{13}$$

When applying Eq. (12) to determine $SV/PSV$, it is also necessary to determine the FAS of the ground acceleration. This study adopted the FAS model proposed by Boore [20] based on the point source theory using various sources, paths, and site parameters. The details of this model can be found in Boore [20] and Zhang and Zhao [27]. The required information regarding various seismological parameters can be found in Boore and Thompson [26], Wang and Rathje [25], and Zhang and Zhao [18]. In addition, Eq. (12) can be decomposed into two terms: the first term (i.e. $\sqrt{\int_0^\infty |Y(\omega)Hv(\omega,\overline{\omega},\xi)|^2 d\omega}/\sqrt{\int_0^\infty |Y(\omega)Hpv(\omega,\overline{\omega},\xi)|^2 d\omega}$) is the ratio of the oscillator-response rms values of SV and PSV, denoted as $R_{\mathrm{rms}}$; The second term (i.e. $Pf_{rv}/Pf_{ra}$) is the ratio of the oscillator-response peak factor between SV and PSV, denoted as $R_{pf}$.

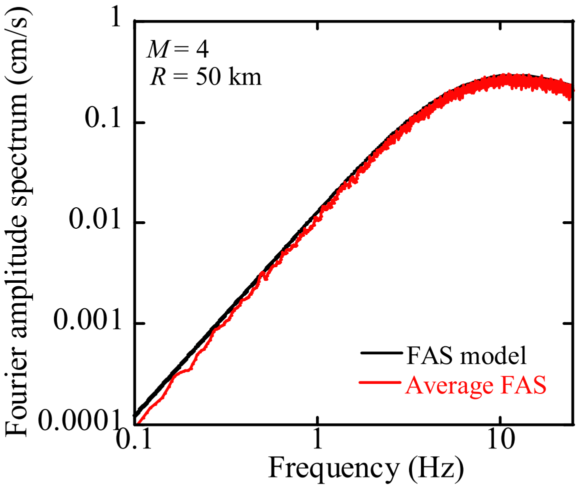


**Fig. 1.** Comparison of the average FAS of the generated time series with the FAS from the point-source model for the cases of $M = 4$ and $R = 50$ km.

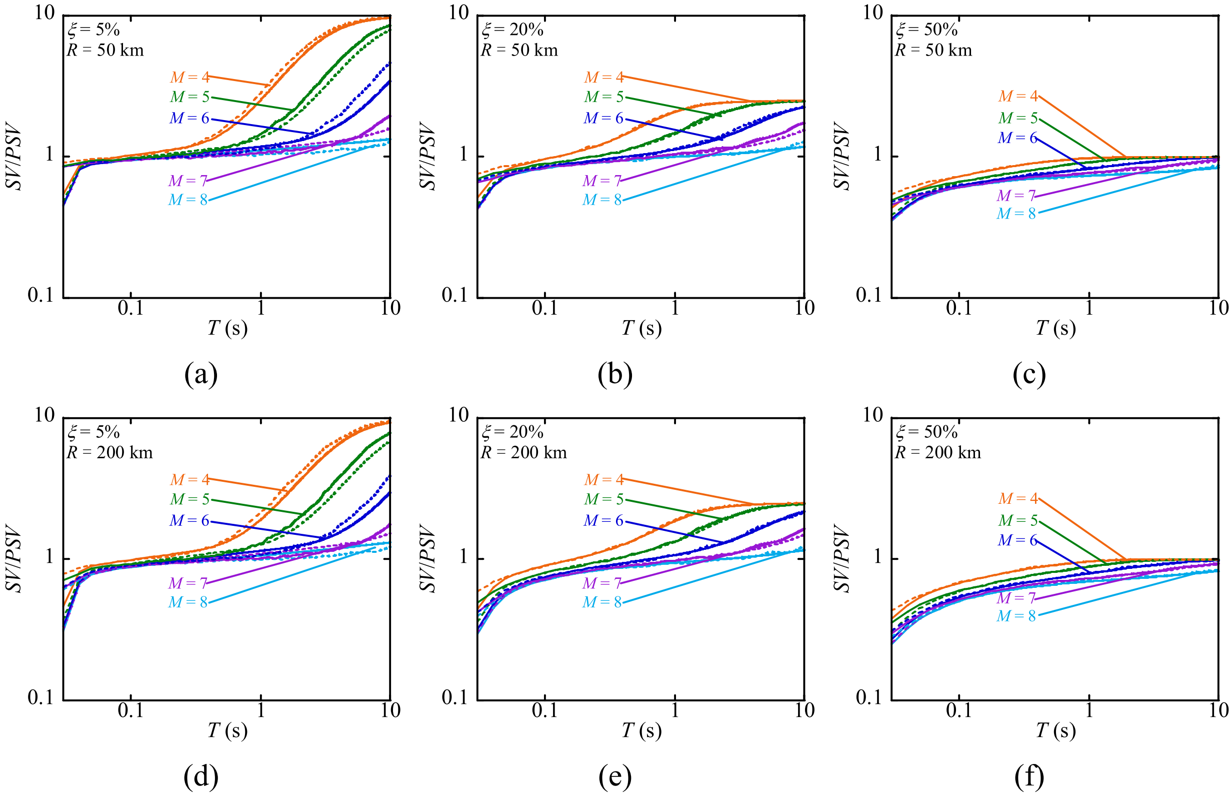


**Fig. 2.** Comparison between *SV*/*PSV* results of proposed approach and time-series analysis, considering various moment magnitudes for cases with (a) $\xi = 5\%$ and $R = 50$ km, (b) $\xi = 20\%$ and $R = 50$ km, (c) $\xi = 50\%$ and $R = 50$ km, (d) $\xi = 5\%$ and $R = 200$ km, (e) $\xi = 20\%$ and $R = 200$ km, and (f) $\xi = 50\%$ and $R = 200$ km. The solid lines represent the results from the proposed approach; the dashed lines represent the results from the time-series analysis.

### *2.2. Comparison with time-series analysis*

To investigate the accuracy of the proposed theoretical equation, its predicted results were compared to those obtained from traditional time-series analysis. The calculations encompass a broad range of the structural parameters, i.e., oscillator periods $T$, range from 0.03 to 10 s, damping ratios $\xi$, range from 5% to 50%, as well as seismological parameters such as moment magnitude $M$, range

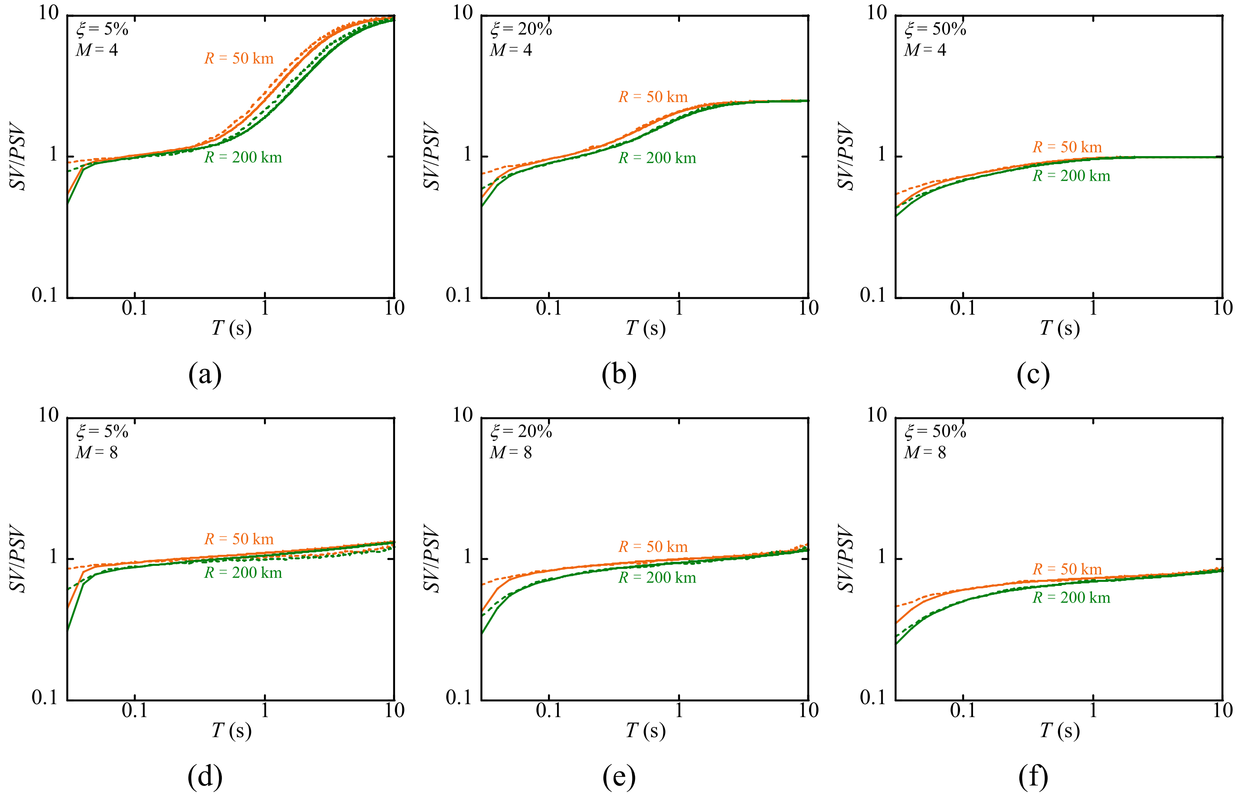


**Fig. 3.** Comparison between *SV/PSV* results of proposed approach and time-series analysis considering different site-to-source distances for cases with (a) $\xi = 5\%$ and $M = 4$, (b) $\xi = 20\%$ and $M = 4$, (c) $\xi = 50\%$ and $M = 4$, (d) $\xi = 5\%$ and $M = 8$, (e) $\xi = 20\%$ and $M = 8$, and (f) $\xi = 50\%$ and $M = 8$. The solid lines represent the results from the proposed approach; the dashed lines represent the results from the time-series analysis.

from 4 to 8, and site-to-source distance $R$, range from 20 to 200 km. The time series used for comparison are generated from the FAS using the Stochastic-Method SIMulation [28] program. For each FAS, a set of 100 time-series accelerations is generated through stochastic simulation [29]; the average FAS of the generated time series is matched with the provided FAS from the point-source model [20]. The average FAS of the generated time series is compared with the FAS from the point-source model for the cases of $M = 4$ and $R = 50$ km in Fig. 1. Subsequently, the values of *SV/PSV* for every generated time series are computed utilizing the direct integration method proposed by Nigam and Jennings [30]. For each FAS, the 100 corresponding results of *SV/PSV* for a provided damping level are averaged and compared with those acquired from the proposed theoretical equation. Some of these representative comparative results were selected and presented in Figs. 2–4.

The presented figures indicate that, although in some cases the results obtained from the proposed theoretical equations are not entirely consistent with those obtained by time series analysis, the level of consistency is high for most cases. The average relative error decreases as the damping ratio increases. For a damping ratio of 5% (Fig. 2(a) and (d)), the average relative error remains around 20% within the period range of 0.05 to 10 s. However, as the damping ratio increases to 50%, it can decrease to only about 2% (Fig. 2(c) and (f)). The good agreement between the proposed theoretical equation and the time series analysis not only validates the accuracy of the proposed theoretical equation but also supports the reasonable assumption in Section 2.1 that the rms durations for SA and SV are the same as SD.

## 3. Relationship between SV and SA based on the derived theoretical equation

### 3.1. Relationship between SV and SA

This section investigates the relationship between SV and SA based on the theoretical equation derived in the previous section. It can be found in Figs. 2–4 that *SV/PSV* is dependent on the oscillator period. The *SV/PSV* values are smaller than unity at short oscillator periods, they increase with the increasing oscillator period. The *SV/PSV* values are close to unity at the intermediate period range, and they may be larger than unity at longer oscillator periods. That indicates that the values of SV are smaller than that of PSV at short oscillator periods, and SV increases relative to the PSV with the increasing oscillator period and may be larger than PSV at longer oscillator periods. In addition, the *SV/PSV* is dependent on the damping ratio, its values decrease with the increasing damping ratio (Fig. 4). Moreover, the *SV/PSV* is dependent on the moment magnitude, its values decrease with the increasing moment magnitude at

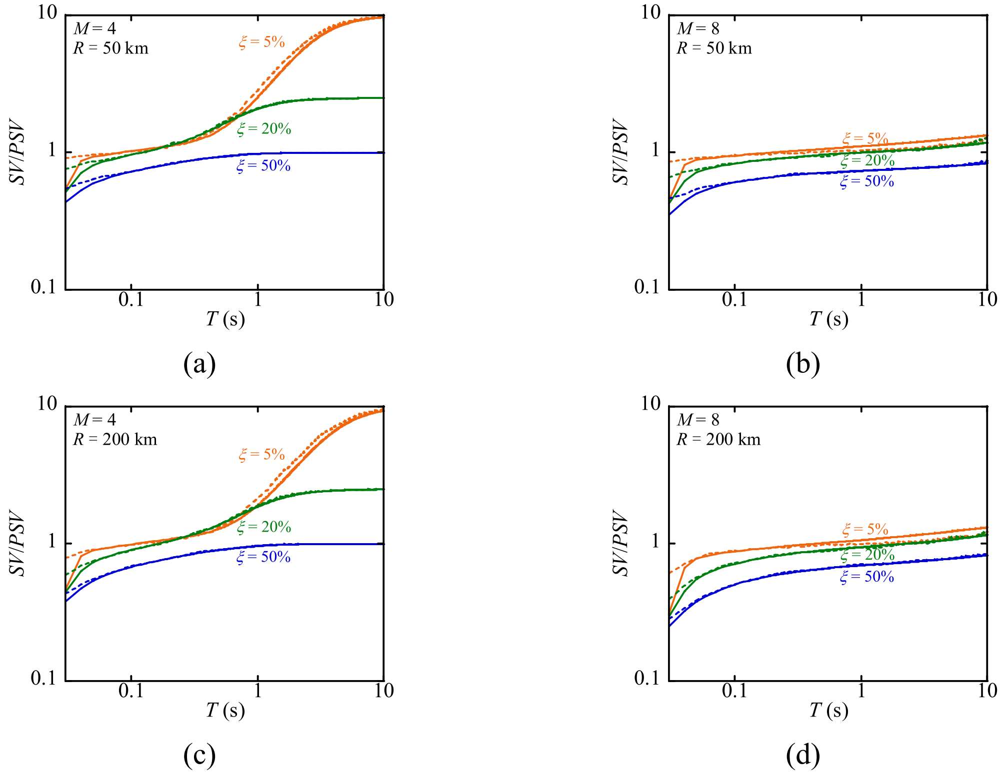


**Fig. 4.** Comparison between *SV/PSV* results of the proposed approach and time-series analysis considering different damping ratios for cases with (a) $M = 4$ and $R = 50$ km, (b) $M = 8$ and $R = 50$ km, (c) $M = 4$ and $R = 200$ km, and (d) $M = 8$ and $R = 200$ km. The solid lines represent the results from the proposed approach; the dashed lines represent the results from the time-series analysis.

most oscillator periods (Fig. 2). However, the difference between SV and PSV does not significantly change with the site-to-source distance, the relationship between SV and PSV is nearly not influenced by site-to-source distance (Fig. 3).

### 3.2. Explanation

To explain the phenomenon observed in Section 3.1, the results of $R_{\mathrm{rms}}$ and $R_{pf}$ in Eq. (12) are calculated and shown in Figs. 5 and 6, respectively. By comparing Fig. 5 and Fig. 2, it is clear that the results of $R_{\mathrm{rms}}$ have a high degree of similarity with those of *SV/PSV*. Fig. 6 shows that the results of $R_{pf}$ are close to unity. These indicate that the trend of *SV/PSV* is primarily determined by $R_{\mathrm{rms}}$, which can facilitate an explanation of the observed relationship based on $R_{\mathrm{rms}}$.

The $R_{\mathrm{rms}}$ is derived from the squared ratio of $\int_0^\infty |Y(\omega)H\nu(\omega,\overline{\omega},\xi)|^2 d\omega$ to $\int_0^\infty |Y(\omega)Hp\nu_{\mathrm{SA}}(\omega,\overline{\omega},\xi)|^2 d\omega$, the $\int_0^\infty |Y(\omega)H\nu(\omega,\overline{\omega},\xi)|^2 d\omega$ on the numerator and the $\int_0^\infty |Y(\omega)Hp\nu_{\mathrm{SA}}(\omega,\overline{\omega},\xi)|^2 d\omega$ on the denominator can be regarded as the areas of the square of the oscillator-response FAS for the SV and PSV, respectively. When the areas for SV and PSV are close, it means that *SV/PSV* is close to unity, while when the area for SV is greater than or smaller than that for PSV, it means that *SV/PSV* is larger or smaller than unity, respectively. Based on Eq. (12), it becomes evident that the discrepancy between the two areas (i.e., two spectra) arises from the discrepancy in the oscillator transfer functions. The values of oscillator transfer functions are represented in Figs. 7, 8, and 9. In these figures, $T_0$ represents the period of FAS corresponding to $\omega$ ($T_0 = 2\pi/\omega$).

From Fig. 7, it can be observed that $|H\nu(\omega,\overline{\omega},\xi)|$ is similar to $|Hp\nu_{\mathrm{SA}}(\omega,\overline{\omega},\xi)|$ around the oscillator period $T$. However, at the periods range of $T_0 < T$, $|H\nu(\omega,\overline{\omega},\xi)| > |Hp\nu_{\mathrm{SA}}(\omega,\overline{\omega},\xi)|$; at the periods range of $T_0 > T$, $|H\nu(\omega,\overline{\omega},\xi)| < |Hp\nu_{\mathrm{SA}}(\omega,\overline{\omega},\xi)|$. Based on the characteristics of $|H\nu(\omega,\overline{\omega},\xi)|$ and $|Hp\nu_{\mathrm{SA}}(\omega,\overline{\omega},\xi)|$, the trends of *SV/PSV* with variation in the oscillator period and damping ratio can be clearly explained. Fig. 8 indicates that when $T$ is short, the period range of $T_0 > T$ is wide, in which $|Hp\nu_{\mathrm{SA}}(\omega,\overline{\omega},\xi)| > |H\nu(\omega,\overline{\omega},\xi)|$. Hence, the area for PSV is larger than that for SV. Therefore, *SV/PSV* is smaller than unity at short oscillator periods, indicating that PSV is larger than SV. As $T$ is increased, the period range of $T_0 < T$ increases, in which $|Hp\nu_{\mathrm{SA}}(\omega,\overline{\omega},\xi)| < |H\nu(\omega,\overline{\omega},\xi)|$. Hence, the area for PSV decreases relative to that for SV. Therefore, *SV/PSV* increases with the increasing oscillator period. When $T$ is increased to some extent, the areas for PSV and SV are similar. Therefore, *SV/PSV* is close to unity at intermediate oscillator periods, indicating that SV and PSV are similar. When $T$ is further increased, the area for PSV may be smaller than that for SV. Therefore, *SV/PSV* may be larger than unity at long oscillator periods, indicating that SV may be larger than PSV. Fig. 9 indicates that as the damping ratio increases, $|Hp\nu_{\mathrm{SA}}(\omega,\overline{\omega},\xi)|$ increases and approaches to $|H\nu(\omega,\overline{\omega},\xi)|$ at the period range of $T_0 < T$, while it remains nearly unchanged at the period range of $T_0 > T$. Hence, the area for PSV relative to that for SV increases with the increasing damping ratio. Therefore, *SV/PSV*

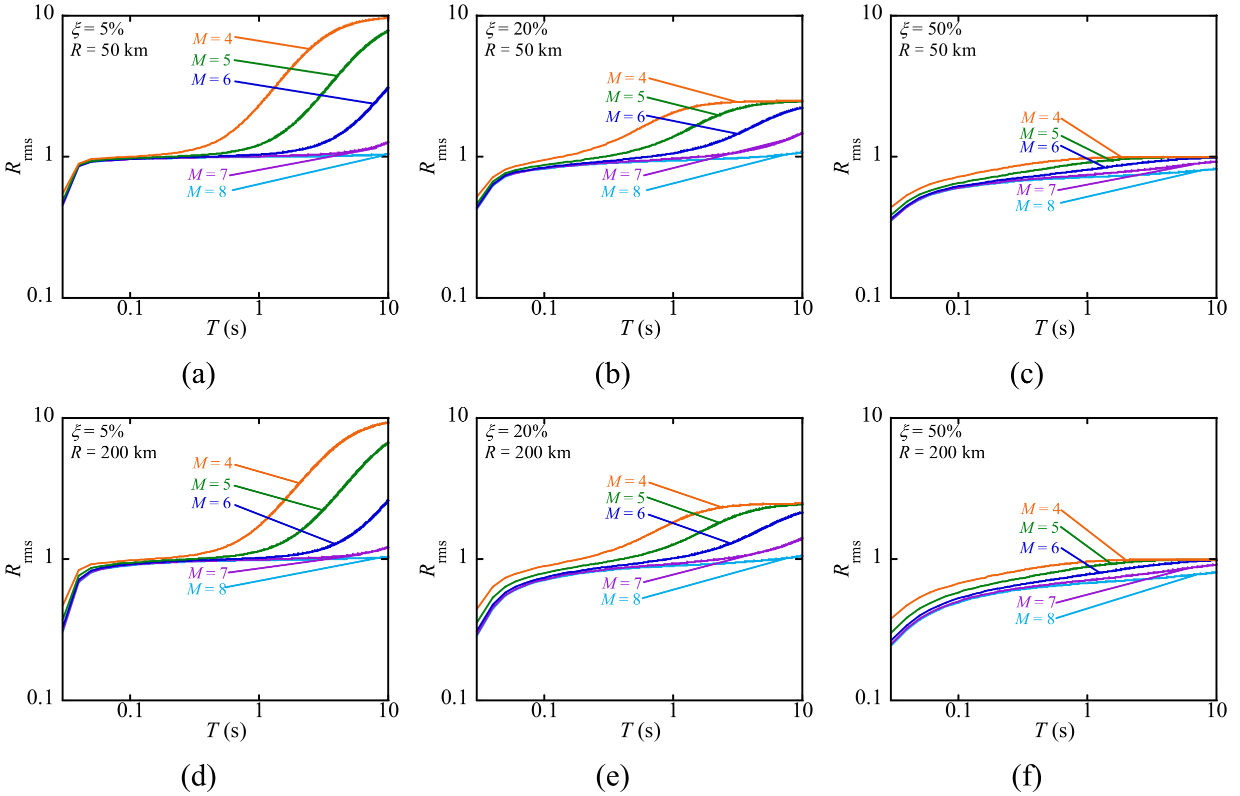


**Fig. 5.** Values of rms ratio $R_{\mathrm{rms}}$ for cases with (a) $\xi = 5\%$ and $R = 50$ km, (b) $\xi = 20\%$ and $R = 50$ km, (c) $\xi = 50\%$ and $R = 50$ km, (d) $\xi = 5\%$ and $R = 200$ km, (e) $\xi = 20\%$ and $R = 200$ km, and (f) $\xi = 50\%$ and $R = 200$ km.

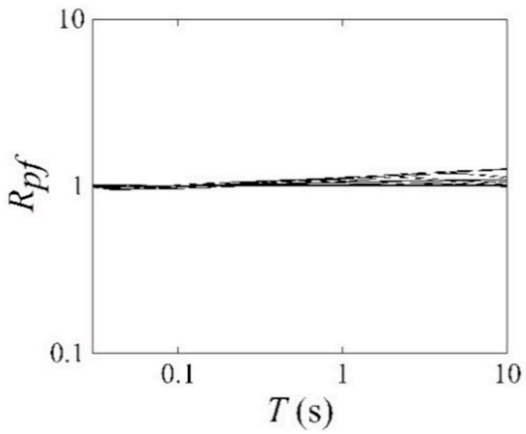


**Fig. 6.** Values of peak-factor ratio $\mathrm{R_{pf}}$ for all cases in Fig. 2.

decreases with the increasing damping ratio.

According to Eq. (5), it is known that the moment magnitude and site-to-source distance influence the variation trend of *SV/PSV* by changing the FAS. Since FAS affects both the numerator and denominator of the $R_{\mathrm{rms}}$, what truly affects *SV/PSV* is its relative value at different periods, rather than its absolute value. Fig. 10 indicates that as the moment magnitude and site-to-source distance increase, the long-period components relatively increase. The values of FAS exhibit a faster increase at long periods compared to short periods (Fig. 10(a)), and it experiences a faster decrease at short periods compared to short periods (Fig. 10(b)). Because $|Hp\nu_{\mathrm{SA}}(\omega, \overline{\varpi}, \xi)| > |H\nu(\omega, \overline{\varpi}, \xi)|$ at long periods, the area for PSV increases relative to that for SV with increasing moment magnitude and site-to-source distance. Therefore, *SV/PSV* decreases with increasing moment magnitude and site-to-source distance. Moreover, the variation in the frequency content with the site-to-source distance is not significant compared to that with moment magnitude (Fig. 10). Therefore, *SV/*

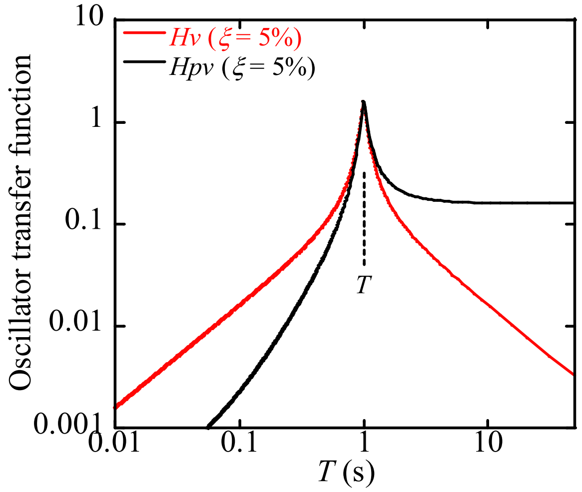


**Fig. 7.** Comparison of oscillator transfer functions for SV and PSV.

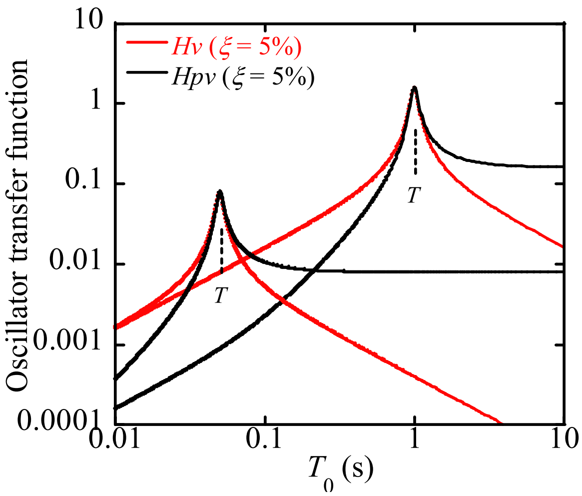


**Fig. 8.** Variation in oscillator transfer functions for SV and PSV with oscillator period.

*PSV* does not significantly change with the site-to-source distance.

## 4. Conversion model from SA to SV

### 4.1. Relationship between SA and SV based on statistical analysis

To confirm the conclusions derived theoretically, a statistical analysis of the relationship between SA and SV was conducted based on a large number of ground motion records. For this purpose, a total of 16,660 horizontal acceleration time histories (8330 seismic ground motions) were collected from the strong-motion seismograph networks (K-NET and KiK-net) of Japan [31–33], which includes a wide range of magnitude $M$ (4–9), epicenter distance $R$ (10–200 km), and site class (classes B, C, D, and E). This paper does not include site class A, because there are few sites belonging to this site class in K-NET and KiK-net. In addition, the hypocenter depth of the chosen seismic data ranges from 0 km to 196 km [34]. The selected earthquakes include both interplate (e.g., 2003 Tokachi earthquake and 2011 off the Pacific coast of Tohoku earthquake) and intraplate earthquakes (e.g., 2000 Tottori earthquake, 2004 Chuetsu earthquake, 2016 Kumamoto earthquakes, and 2018 Hokkaido Eastern Iburi earthquake). The collected records in each site class are classified into three groups based on magnitude $M$: $4 \leq M < 5.5$, $5 \leq M < 6.5$, and $M \geq 6.5$. Each group is further divided into three subgroups based on the epicenter distance $R$: $10 \leq R < 50$ km, $50 \leq R < 100$ km, and $100 \leq R \leq 200$ km. There are 36 groups, the details of which can be found in Hang *et al.* [19] and Zhang and Zhao [33].

Additionally, a baseline adjustment is applied to all records to remove long-period noise. Ideally, each ground motion record should also be processed to filter out frequencies with unacceptable low signal-to-noise ratios and used only within the available frequency

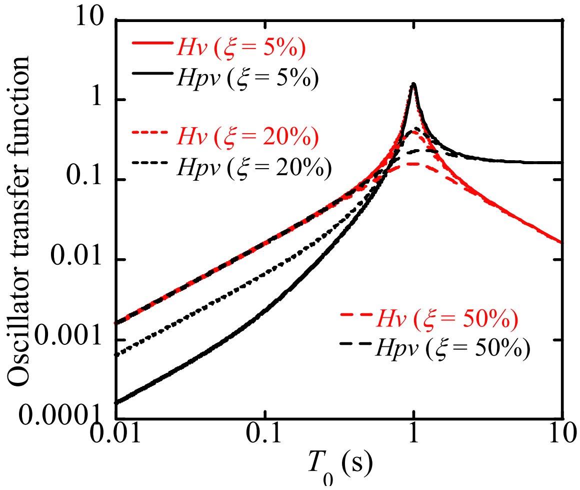


**Fig. 9.** Variation in oscillator transfer functions for SV and PSV with damping ratio.

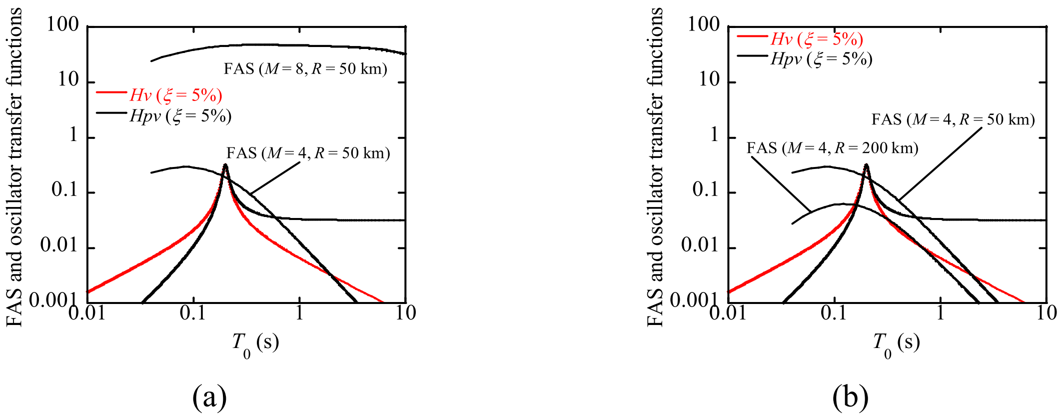


**Fig. 10.** Effects of (a) moment magnitude and (b) site-to-source distance on FAS.

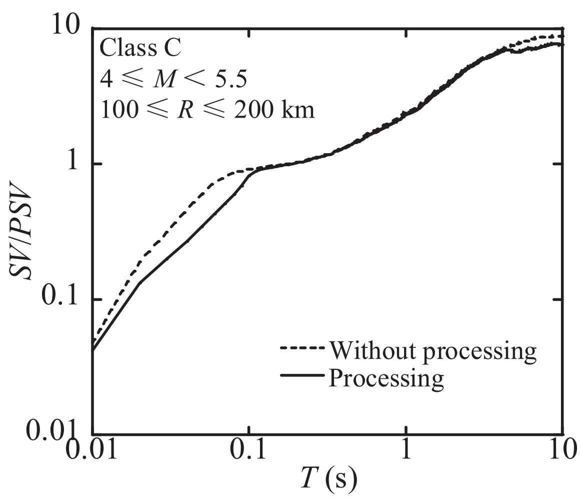


**Fig. 11.** Comparison between the *SV/PSV* results with and without processing the ground motion records.

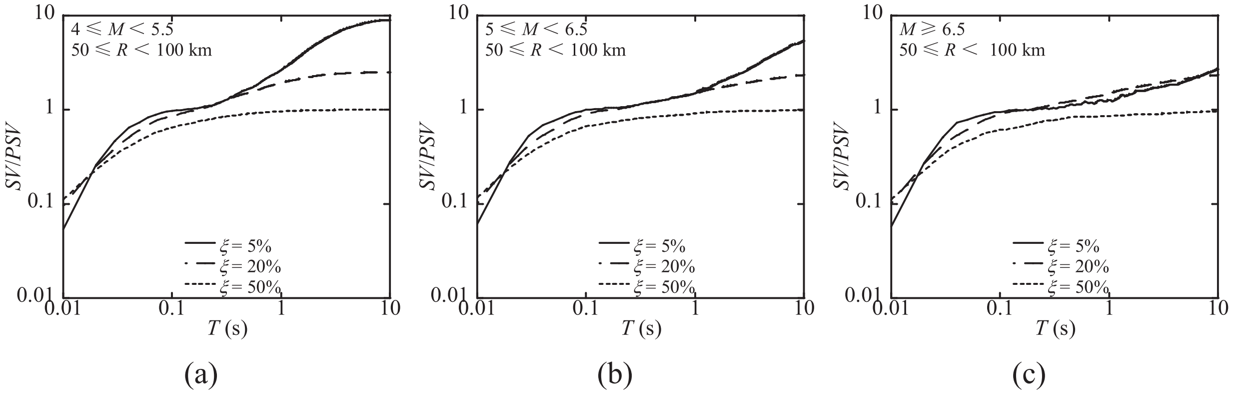


**Fig. 12.** *SV/PSV* with different damping ratios in Class B.

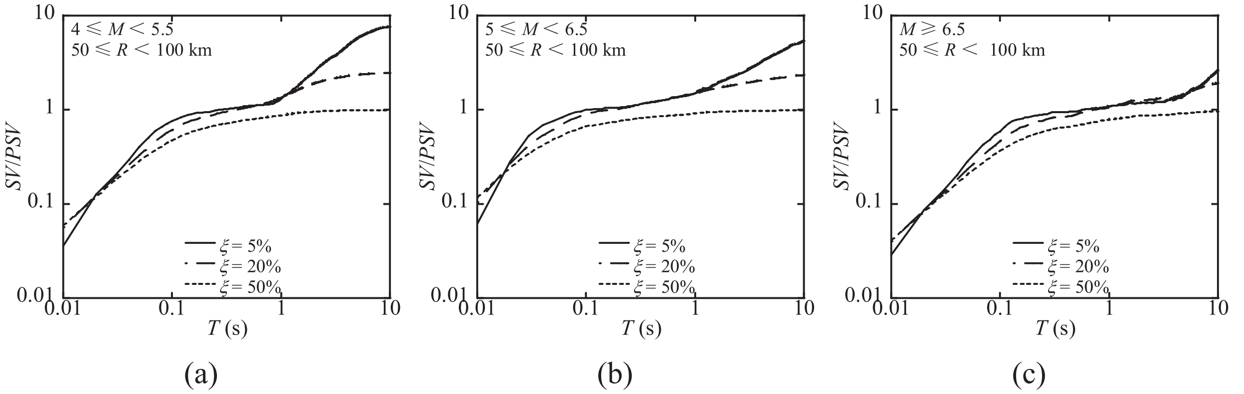


**Fig. 13.** *SV/PSV* with different damping ratios in Class E.

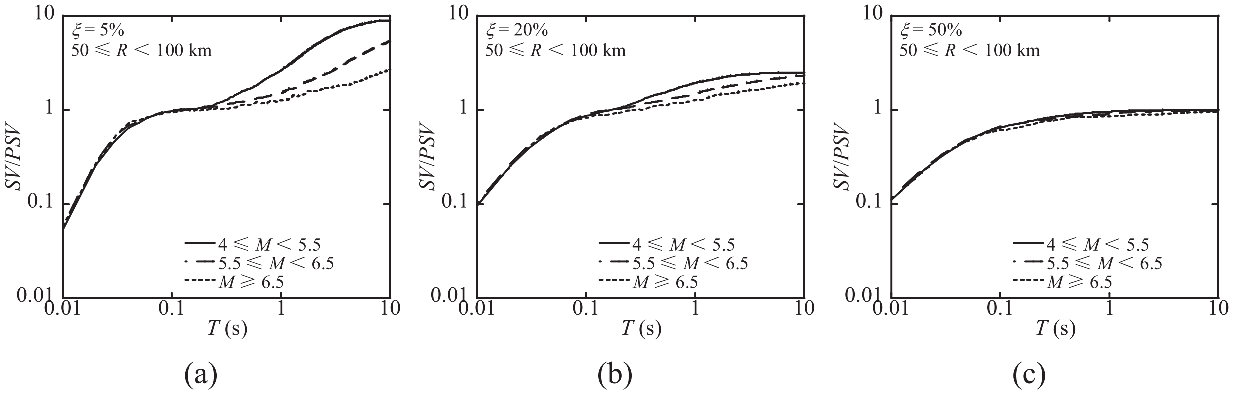


**Fig. 14.** *SV/PSV* with different magnitudes in Class B.

range. However, since this study focuses on the *SV/PSV* ratio, it is assumed that the noise present in both SV and PSV can be negated through the calculation of this ratio. To validate this assumption, a comparison was made between the *SV/PSV* results with and without processing the ground motion records, as shown in Fig. 11. The group with the smallest magnitudes ($4 \leq M < 5.5$) and the largest distances ($100 \leq R \leq 200$ km) in site class C, which may be mostly affected by noise, were selected for the comparison. The automatic P-phase arrival-time picker developed by Kalkan [35] was used to identify the noise window, and the method by Bahrampouri *et al.* [36] was employed to filter out frequencies with unacceptable low signal-to-noise ratios. As observed in Fig. 11, there is no significant difference between the *SV/PSV* results with and without the ground motion records being processed, particularly within the first 6 s. The average relative difference between the two within this period is only 5.9%. Thus, filtering out frequencies with unacceptable low

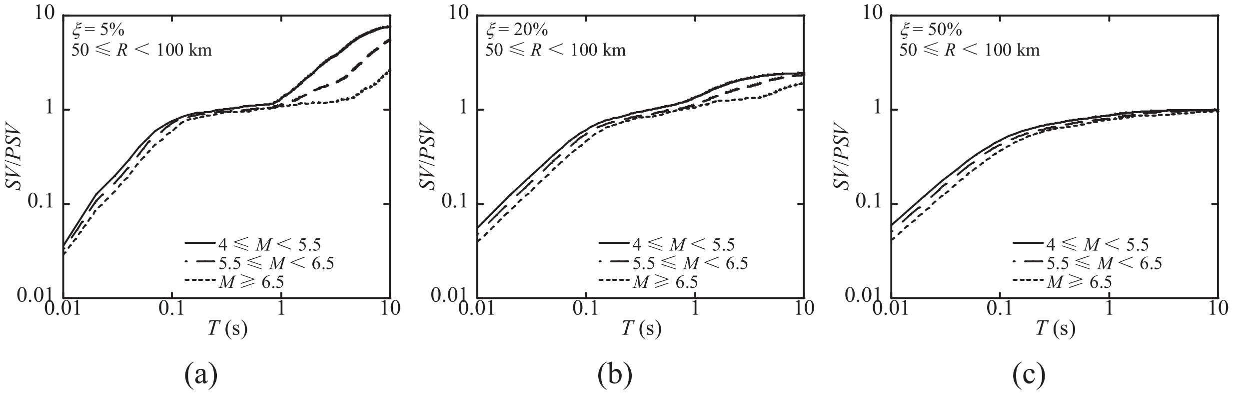


**Fig. 15.** *SV/PSV* with different magnitudes in Class E.

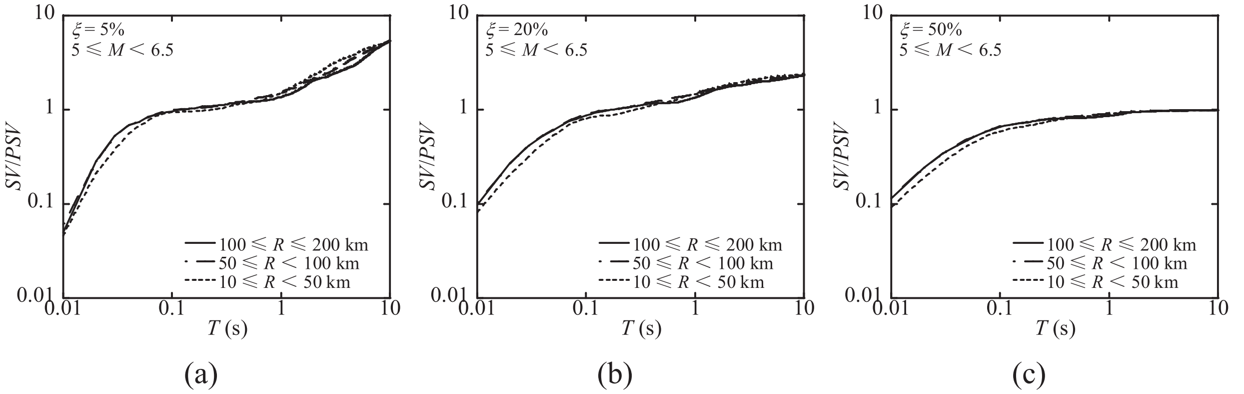


**Fig. 16.** *SV/PSV* with different distances in Class B.

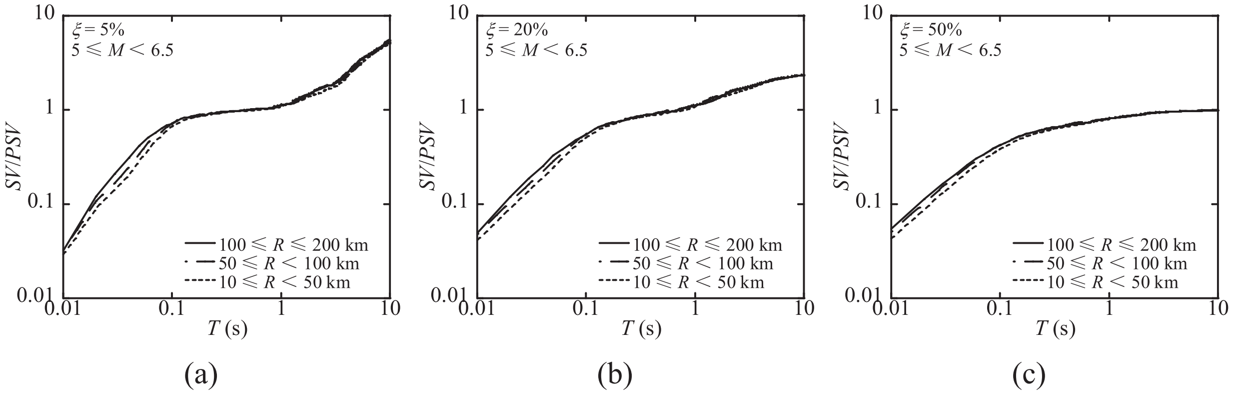


**Fig. 17.** *SV/PSV* with different distances in Class E.

signal-to-noise ratios has no significant impact on the *SV/PSV* ratio. Consequently, ground motion records were not processed further, except for the baseline adjustment.

The SV and PSV of the collected records are calculated considering oscillator periods ranging from 0.01 s to 10 s (interval 0.01 s) and damping ratios of 5%, 10%, 20%, 30%, 40%, and 50%. The considered oscillator periods and damping ratios are similar to those discussed in Section 2.2. Then, the results of *SV/PSV* for each group are averaged, and some of them are selected as representatives and presented in Figs. 12–20. Figs. 12 and 13 present the results of *SV/PSV* with different damping ratios in site classes B and E, respectively. Figs. 14 and 15 compare the results of *SV/PSV* with different magnitudes in site classes B and E, respectively. Figs. 16 and 17 compare the results of *SV/PSV* with different epicenter distances in site classes B and E, respectively. Figs. 18, 19, and 20 compare

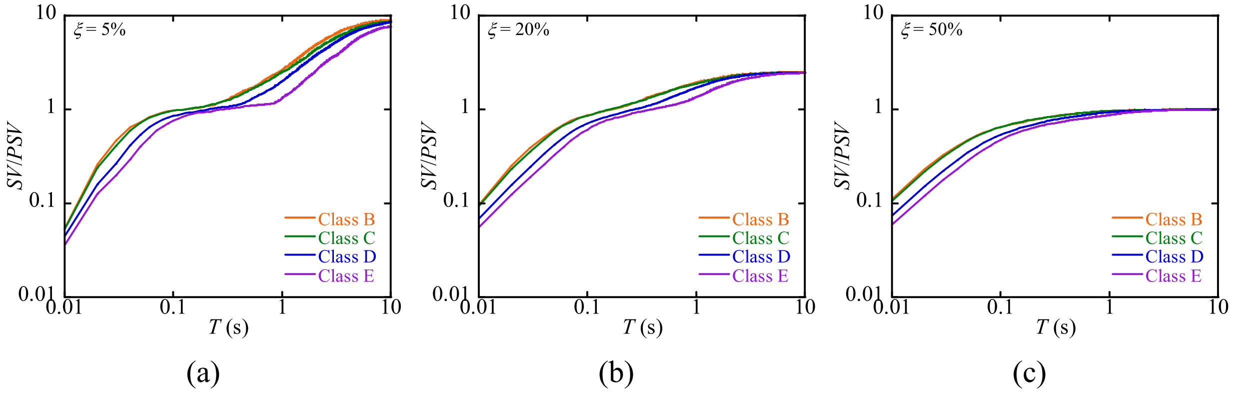


**Fig. 18.** *SV/PSV* in different site classes for magnitudes of $4 \leq M < 5.5$.

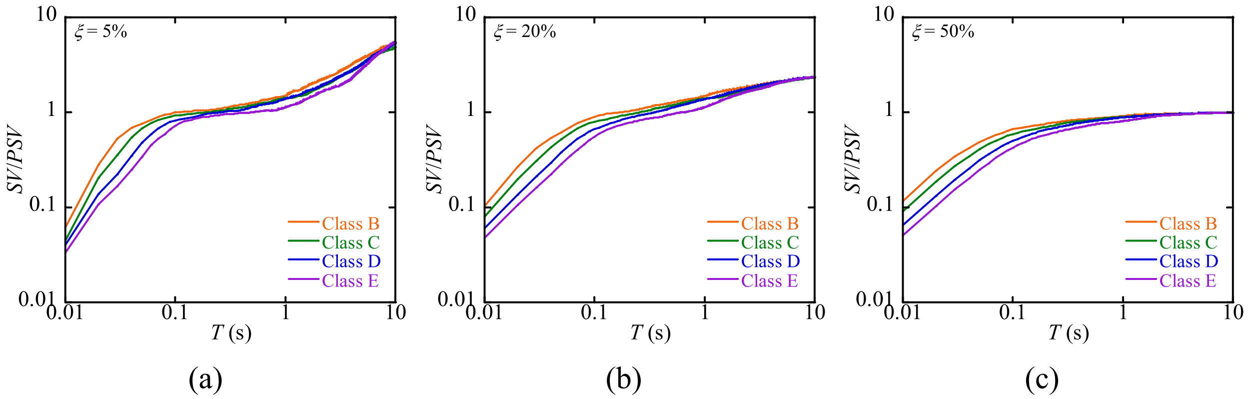


**Fig. 19.** *SV/PSV* in different site classes for magnitudes of $5 \leq M < 6.5$.

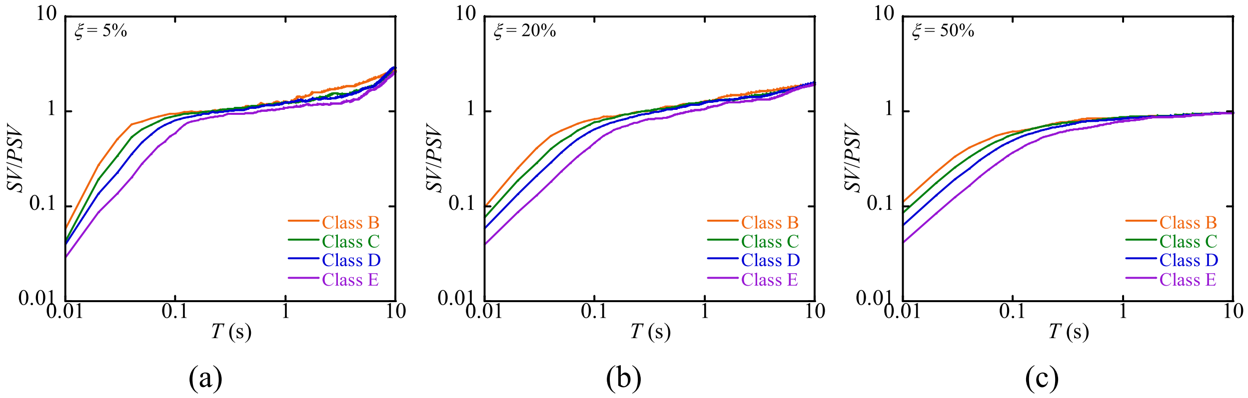


**Fig. 20.** *SV/PSV* in different site classes for magnitudes of $M \geq 6.5$.

the results of *SV/PSV* in different site classes. It can be observed from these figures that the variation trend of *SV/PSV* with the oscillator period is consistent with that based on the theoretical equation. The SV and PSV are similar at the intermediate period range, and the SV is smaller than PSV at short oscillator periods, and larger than PSV at longer oscillator periods. In addition, the variation trends of the *SV/PSV* with damping ratio, magnitude, and epicenter distance, are consistent with those derived theoretically in section 2.2.

The site effects on *SV/PSV* are not discussed in Section 2, because the proposed theoretical relationship does not involve the site class term. Figs. 18, 19, and 20 show that the *SV/PSV* is also influenced by site class. The *SV/PSV* gradually decreases as the site class varies from B to E at short oscillator periods, while *SV/PSV* is nearly constant with the variation of site class at long oscillator periods. This means that the difference between SV and PSV increases as the site varies from hard rock to soft soil at short oscillator periods.

**Table 1**
Values of regression coefficients in Eqs. (14) – (17).

| | B | C | D | E |
|---|---|---|---|---|
| $b$ | 0.65 | 0.75 | 0.85 | 0.95 |
| $e_1$ | 1.18 | 0.91 | 0.83 | 0.57 |
| $e_2$ | −0.77 | −0.73 | −0.64 | −0.53 |
| $e_3$ | 0.01 | 0.05 | 0.04 | 0.06 |
| $f_1$ | −0.45 | −0.28 | −0.36 | −0.36 |
| $f_2$ | 0.37 | 0.23 | 0.29 | 0.29 |
| $f_3$ | −0.07 | −0.05 | −0.06 | −0.05 |
| $f_4$ | 4.26 | 2.43 | 2.98 | 2.79 |
| $f_5$ | −3.41 | −1.96 | −2.32 | −2.12 |
| $f_6$ | 0.67 | 0.39 | 0.43 | 0.39 |
| $f_7$ | −9.07 | −4.31 | −4.92 | −4.03 |
| $f_8$ | 7.20 | 3.37 | 3.73 | 2.93 |
| $f_9$ | −1.40 | −0.66 | −0.69 | −0.54 |
| $g_1$ | 0.96 | 0.64 | 0.86 | 0.78 |
| $g_2$ | −0.74 | −0.51 | −0.64 | −0.59 |
| $g_3$ | 0.13 | 0.10 | 0.10 | 0.10 |
| $g_4$ | −7.99 | −4.67 | −6.25 | −5.07 |
| $g_5$ | 5.99 | 3.55 | 4.43 | 3.68 |
| $g_6$ | −0.98 | −0.65 | −0.62 | −0.59 |
| $g_7$ | 15.04 | 6.51 | 9.05 | 5.78 |
| $g_8$ | −11.30 | −4.93 | −6.26 | −4.15 |
| $g_9$ | 1.92 | 1.08 | 1.00 | 0.97 |

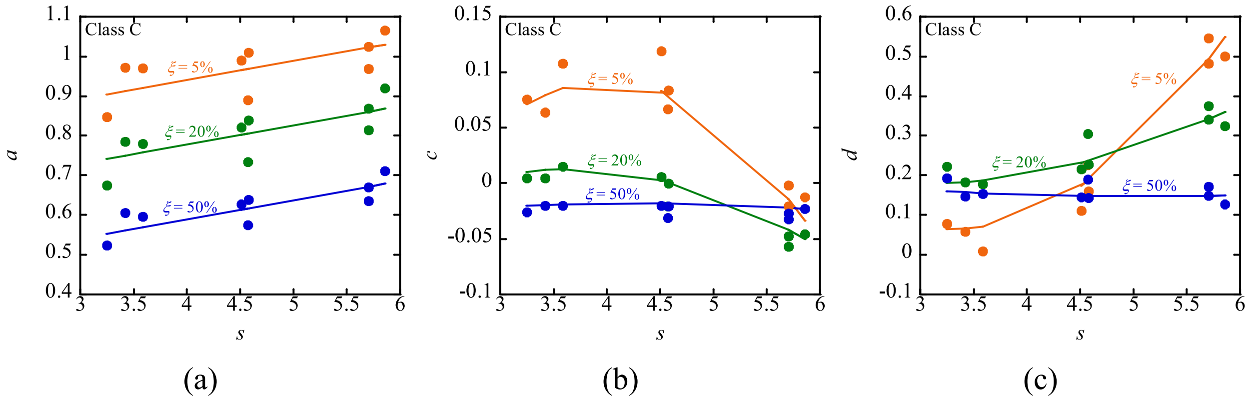


**Fig. 21.** Comparison of the results of $a$, $c$, and $d$ obtained by Eqs. (15) – (17) with those derived from actual ground motion records using the SV/PSV model expressed by Eq. (14). The circles represent results from actual ground motion records; the lines represent results from Eqs. (15) – (17).

### 4.2. Proposed model

To establish a simple model for transforming the SA to the SV, regression analysis is conducted based on the selected ground motion records. Because the *SV/PSV* performs differently before and after around a period of 0.1 s, $T = 0.1$ s was chosen as the dividing point. Numerous functional forms were explored to match the *SV/PSV* values. Ultimately, considering a balance between accuracy and simplicity, a simple *SV/PSV* model was proposed as follows:

$$SV/PSV_{\mathrm{SA}} = \begin{cases} a\left(\dfrac{T}{0.1}\right)^{b} & T \leq 0.1 \\ a\left(\dfrac{T}{0.1}\right)^{(c\ln(T)+d)} & T > 0.1 \end{cases} \tag{14}$$

in which $a$, $b$, $c$, and $d$ are coefficients regressed nonlinearly based on the least squares method. The values of $b$ in different sites are shown in Table 1. The regression coefficients $a$, $c$, and $d$ are found to be related to magnitude, distance, site class, and damping ratio. However, due to the lack of specific information about magnitude and distance in the seismic code, it needs to determine a coefficient to represent the impact of these seismological parameters, and this parameter can be derived from the seismic code. Zhang and Zhao [34] introduced a response spectrum shape coefficient to represent the impact of these seismological parameters. By conducting a correlation analysis, it is found that the response spectrum shape coefficient has a good positive correlation with magnitudes and

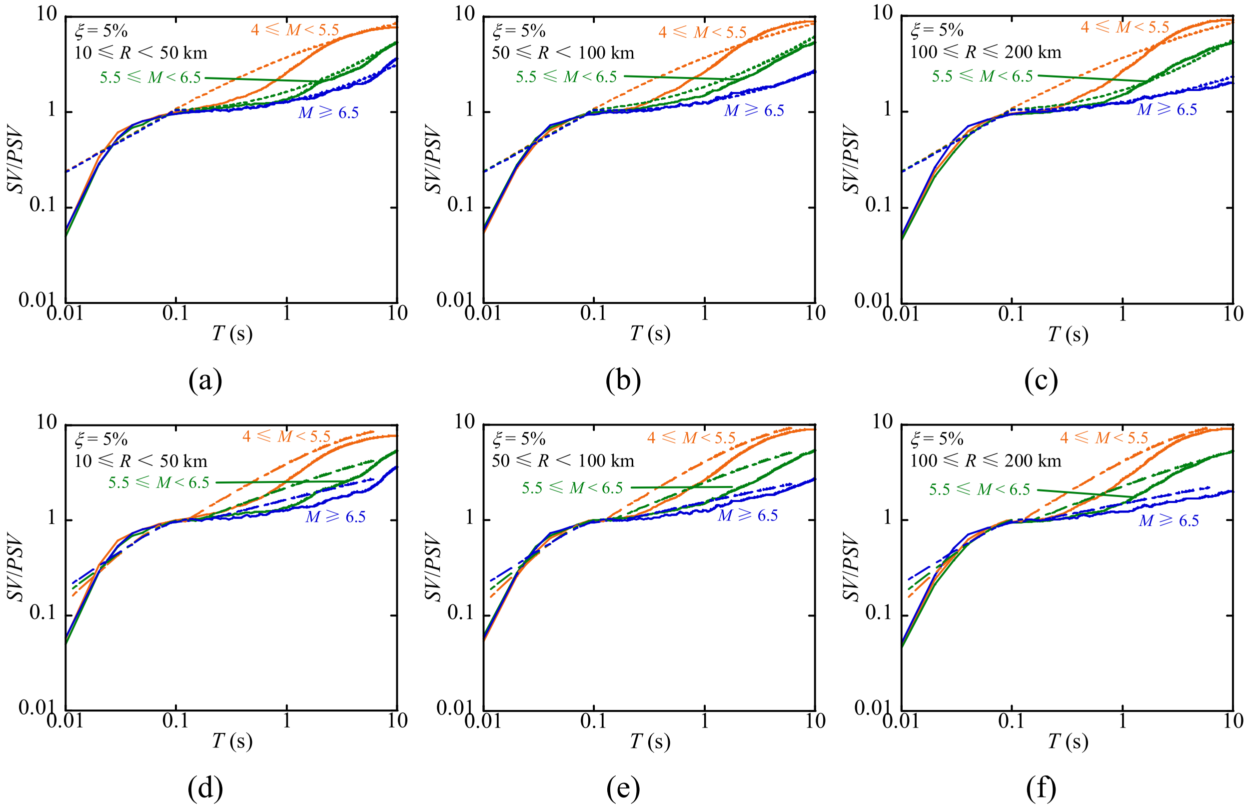


**Fig. 22.** Comparison of the *SV/PSV* results obtained by the proposed model with those of ground motion records and a previous model considering a damping ratio of 5% in Class B for magnitudes of (a) $10 \le R < 50$ km, (b) $50 \le R < 100$ km, (c) $100 \le R \le 200$ km. The solid lines represent the results from the proposed approach; the dashed lines represent the results from actual ground motion records; the dash-dot lines represent the results obtained from the hybrid model combining Liu *et al.* [15] and Hang *et al.* [19].

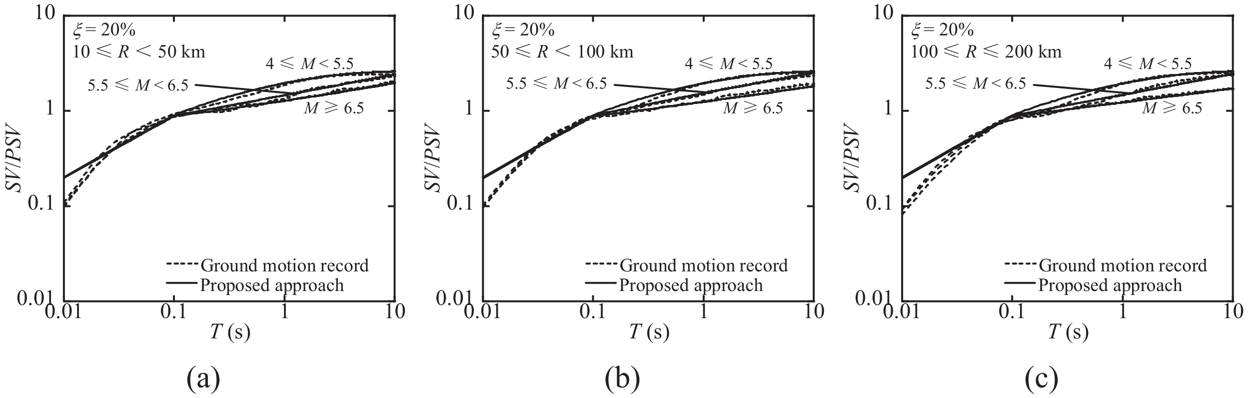


**Fig. 23.** Comparison of the *SV/PSV* results obtained by the proposed model and those of ground motion records considering a damping ratio of 20% in Class B for magnitudes of (a) $10 \le R < 50$ km, (b) $50 \le R < 100$ km, (c) $100 \le R \le 200$ km.

distances in each site class. However, when the correlation analysis is performed by mixing the results of all the site classes, correlations between the response spectrum shape coefficient with magnitudes and distances become poor. Therefore, the coefficients $a$, $c$, and $d$ were regressed separately for each site class. The expressions for regression coefficients $a$, $c$, and $d$ are constructed using the coefficient $s$, as follows:

$$a = e_1 + e_2\xi^{0.5} + e_3 s \tag{15}$$

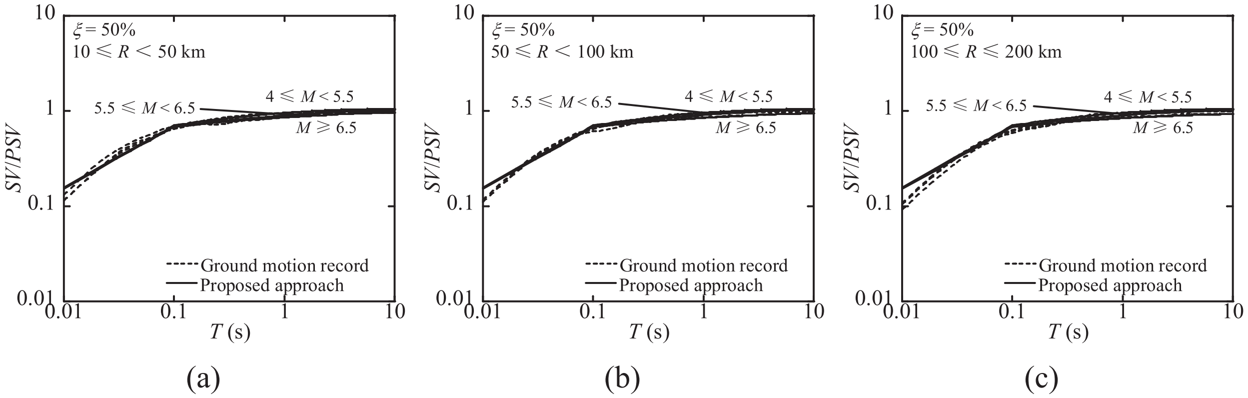


**Fig. 24.** Comparison of the *SV/PSV* results obtained by the proposed model and those of ground motion records considering a damping ratio of 50% in Class B for magnitudes of (a) $10 \leq R < 50$ km, (b) $50 \leq R < 100$ km, (c) $100 \leq R \leq 200$ km.

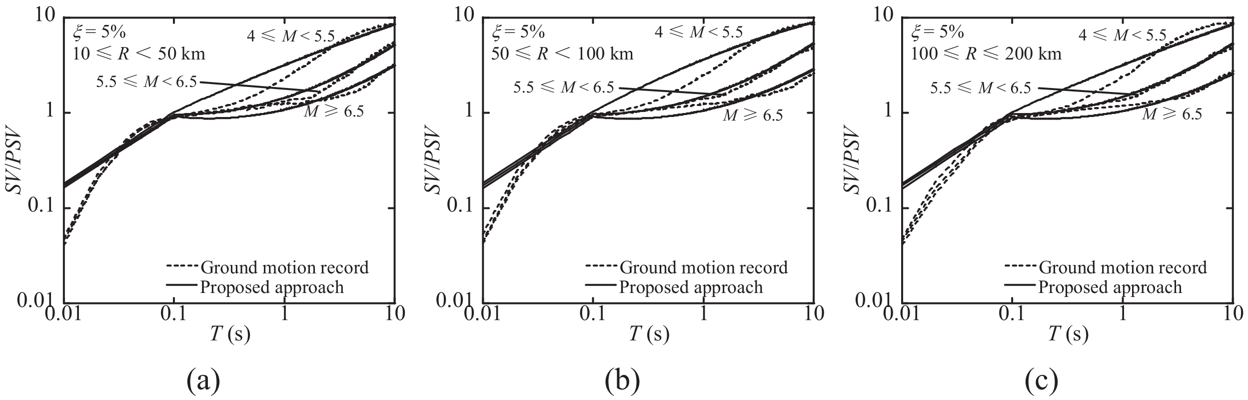


**Fig. 25.** Comparison of the *SV/PSV* results obtained by the proposed model and those of ground motion records considering a damping ratio of 5% in Class C for magnitudes of (a) $10 \leq R < 50$ km, (b) $50 \leq R < 100$ km, (c) $100 \leq R \leq 200$ km.

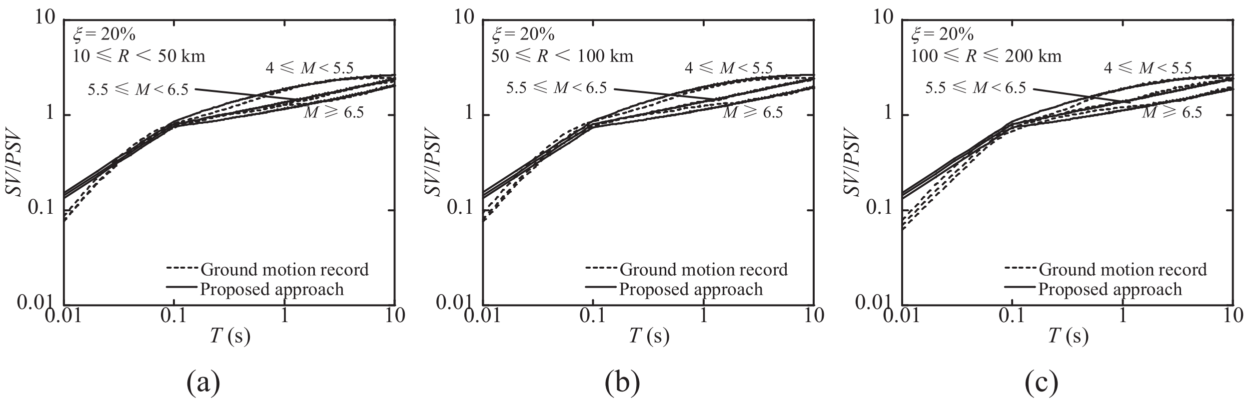


**Fig. 26.** Comparison of the *SV/PSV* results obtained by the proposed model and those of ground motion records considering a damping ratio of 20% in Class C for magnitudes of (a) $10 \leq R < 50$ km, (b) $50 \leq R < 100$ km, (c) $100 \leq R \leq 200$ km.

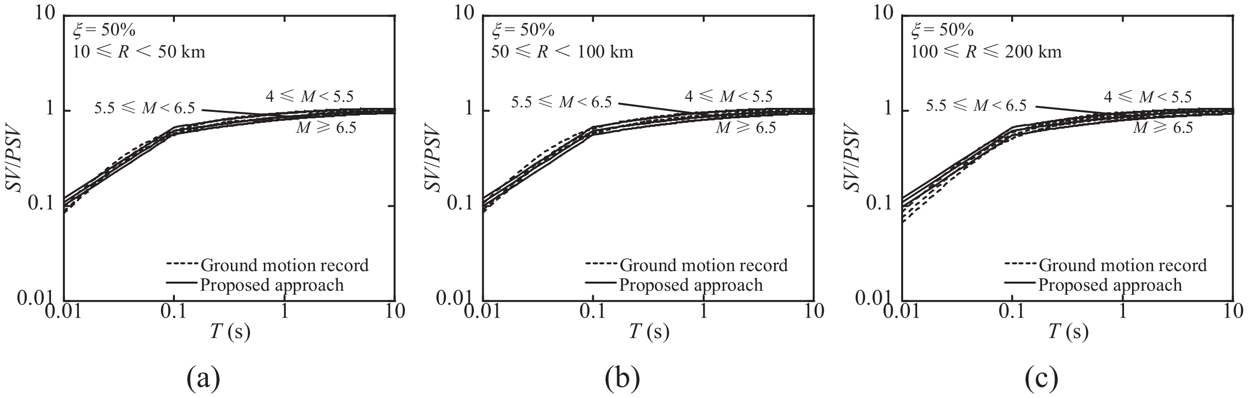


**Fig. 27.** Comparison of the *SV/PSV* results obtained by the proposed model and those of ground motion records considering a damping ratio of 50% in Class C for magnitudes of (a) $10 \le R < 50$ km, (b) $50 \le R < 100$ km, (c) $100 \le R \le 200$ km.

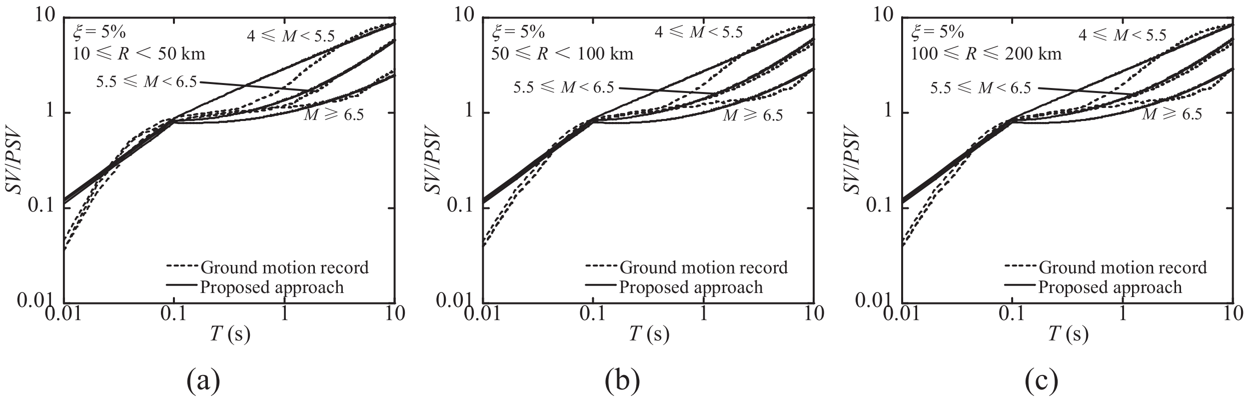


**Fig. 28.** Comparison of the *SV/PSV* results obtained by the proposed model and those of ground motion records considering a damping ratio of 5% in Class D for magnitudes of (a) $10 \le R < 50$ km, (b) $50 \le R < 100$ km, (c) $100 \le R \le 200$ km.

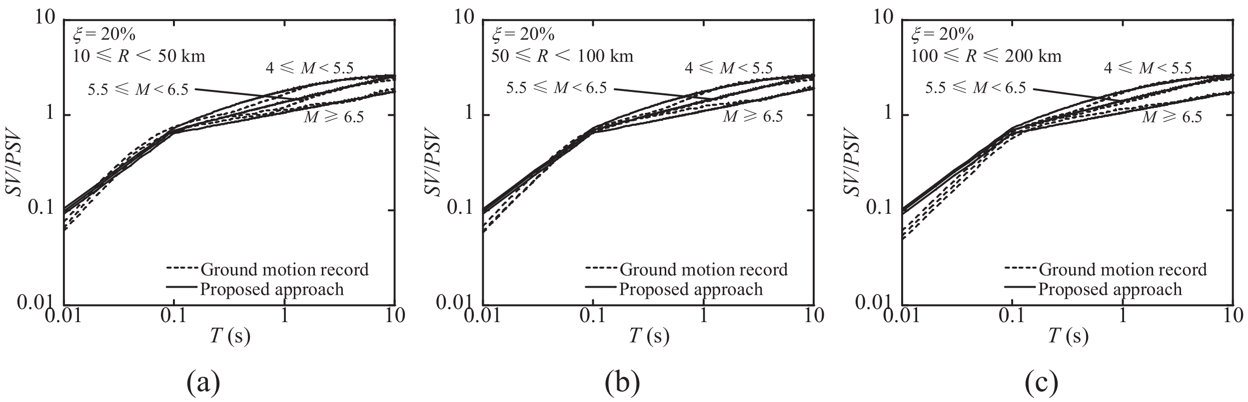


**Fig. 29.** Comparison of the *SV/PSV* results obtained by the proposed model and those of ground motion records considering a damping ratio of 20% in Class D for magnitudes of (a) $10 \le R < 50$ km, (b) $50 \le R < 100$ km, (c) $100 \le R \le 200$ km.

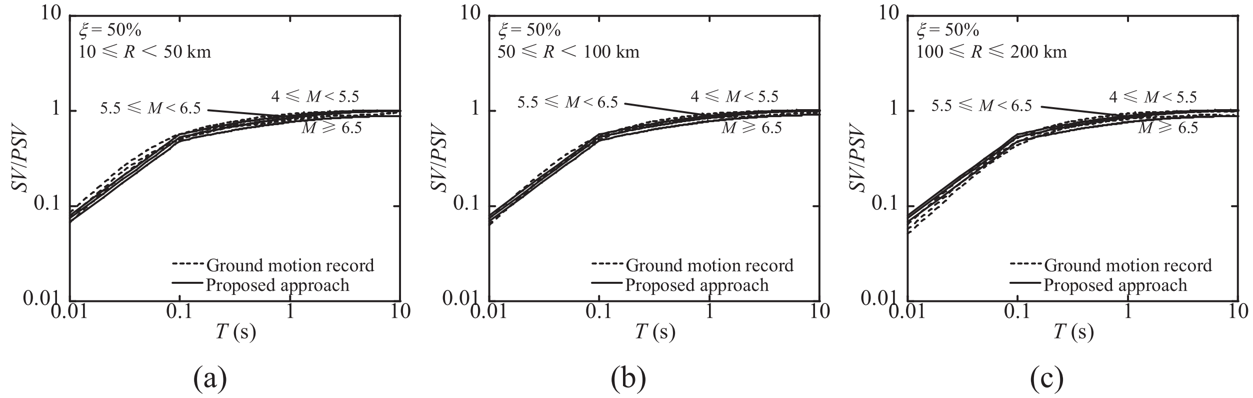


**Fig. 30.** Comparison of the *SV/PSV* results obtained by the proposed model and those of ground motion records considering a damping ratio of 50% in Class D for magnitudes of (a) $10 \leq R < 50$ km, (b) $50 \leq R < 100$ km, (c) $100 \leq R \leq 200$ km.

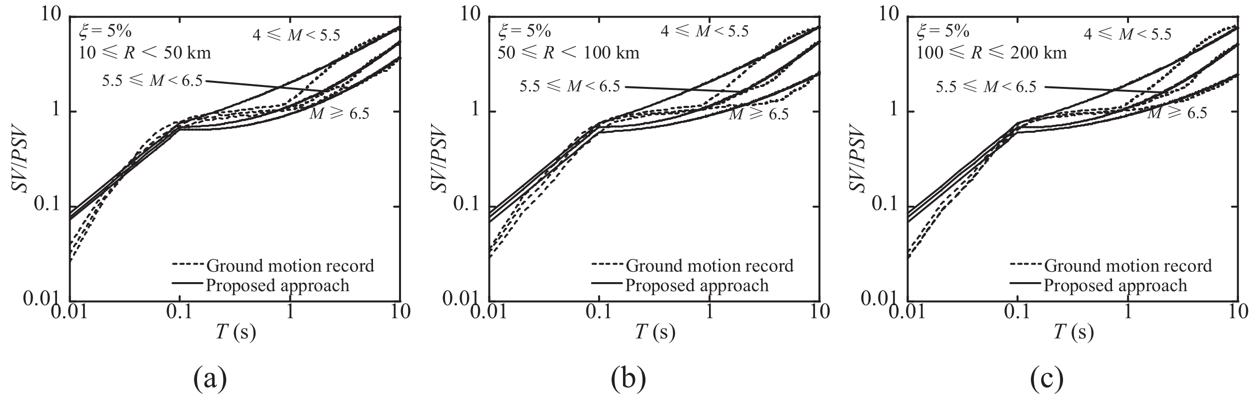


**Fig. 31.** Comparison of the *SV/PSV* results obtained by the proposed model and those of ground motion records considering a damping ratio of 5% in Class E for magnitudes of (a) $10 \leq R < 50$ km, (b) $50 \leq R < 100$ km, (c) $100 \leq R \leq 200$ km.

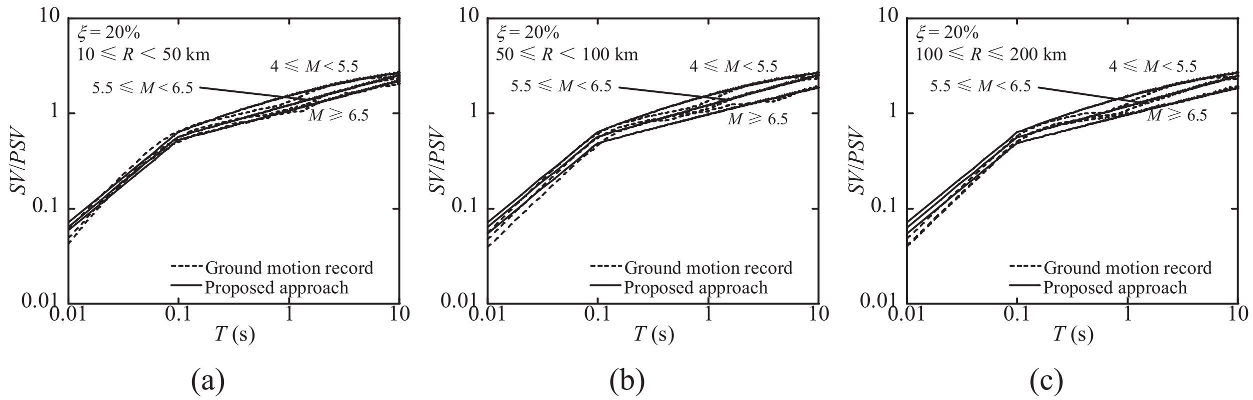


**Fig. 32.** Comparison of the *SV/PSV* results obtained by the proposed model and those of ground motion records considering a damping ratio of 20% in Class E for magnitudes of (a) $10 \leq R < 50$ km, (b) $50 \leq R < 100$ km, (c) $100 \leq R \leq 200$ km.

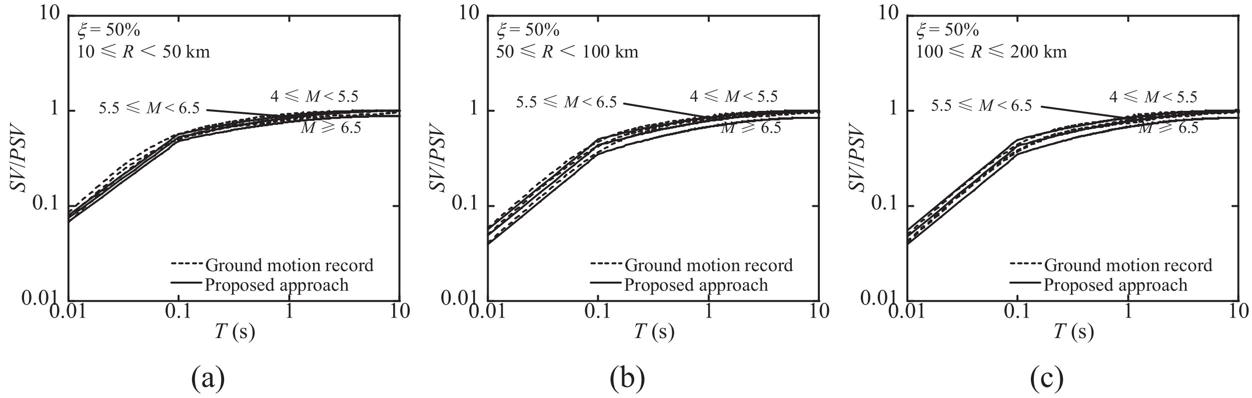


**Fig. 33.** Comparison of the *SV/PSV* results obtained by the proposed model and those of ground motion records considering a damping ratio of 50% in Class E for magnitudes of (a) $10 \le R < 50$ km, (b) $50 \le R < 100$ km, (c) $100 \le R \le 200$ km.

$$c = (f_1\xi^2 + f_2\xi + f_3)s^2 + (f_4\xi^2 + f_5\xi + f_6)s + (f_7\xi^2 + f_8\xi + f_9) \tag{16}$$

$$d = (g_1\xi^2 + g_2\xi + g_3)s^2 + (g_4\xi^2 + g_5\xi + g_6)s + (g_7\xi^2 + g_8\xi + g_9) \tag{17}$$

where $e_1 - e_3, f_1 - f_9$, and $g_1 - g_9$, are coefficients regressed nonlinearly based on the least squares method, they depend on site classes, as listed in Table 1. Fig. 21 compares the results of $a$, $c$, and $d$ obtained by Eqs. (15) – (17) with those derived from actual ground motion records using the *SV/PSV* model expressed by Eq. (14). The $s$ is the response spectrum shape coefficient, which is expressed as:

$$s = \ln\left(\frac{SA(6\text{s})}{PGA}\right) \tag{18}$$

in which, $SA(6\text{s})$ and $PGA$ are the values of SA at 6 s and 0 s, respectively. As can be seen from Eq. (18), the coefficient $s$ can be easily derived from the SA specified in the seismic code.

### 4.3. Comparison between the proposed model and measured values

To investigate the accuracy of the proposed model for transforming SA to SV, its predicted results were compared with values of actual ground motion records. The results with damping ratios of 5%, 20%, and 50% in different classes are selected as representative, as shown in Figs. 22–33. It can be found that the results of the proposed model agree very well with those obtained from actual ground motion records. The coefficient of determination $R^2$ is used to evaluate the agreement of the results, and the closer it is to 1, the higher the agreement of the results. The $R^2$ calculated in this paper can be greater than 0.97. In addition, the agreement of the proposed model increases with the increase of the damping ratio. The average relative error at 0.01–10 s is around 17% for cases with a damping ratio of 5%, while it decreases to only about 1.4% when the damping ratio increases to 50%. The results of other damping ratios not shown, such as 10%, 30%, and 40%, also have a high degree of agreement. The proposed model for transforming SA to SV applies to the Japanese region, and its applicability to other regions has not been discussed in this paper and will be further studied in future work.

In addition, the proposed model for transforming SA to SV was compared with a previous model. Although there is no direct conversion model from SA to SV, a combination of the *SA/PSA* model of Hang *et al.* [19] and the $SV/PSV_{SD}$ model of Liu *et al.* [15] can be used to convert SA to SV. Representative results of *SV/PSV* by the hybrid model are shown in Fig. 22. The accuracy of the hybrid model (Fig. 22(d) – (f)) is significantly lower than that of the proposed model (Fig. 22(a) – (c)), especially for the cases with moderate and large magnitudes. For example, the average relative error of the hybrid model at 0.01–6 s is 43.17% for the moderate magnitude case in Fig. 22(e), whereas the proposed model shows an average relative error of only 14.35% for the corresponding case in Fig. 22(b). For the large magnitude case in Fig. 22(f), the hybrid model's average relative error at 0.01–6 s is 15.7%, while the proposed model's average relative error is only 3.32% for the corresponding case in Fig. 22(c). More importantly, *SA/PSA* model by Hang *et al.* [19] is impractical for structural analysis because it requires information on magnitude and distance, which are not typically provided in seismic codes. Although the calculations presented in Fig. 22 assume that this information is known, the hybrid model is considered not feasible for practical applications at the present stage.

## 5. Conclusions

This study developed a theoretical equation to systematically investigate structural and seismological parameters' effects on the SA-SV relationship, based on random vibration theory. The theoretical conclusions were confirmed based on regression analysis of a large number of ground motion records, and a model to convert SA to SV was established based on this analysis. The main conclusions of this study can be briefly summarized as follows:

(1) The comparison of the *SV/PSV* results of the proposed theoretical equation with those of traditional time series analysis shows that the equation is valid and has a high degree of agreement.

(2) The relationship between SA and SV is dependent on the oscillator period, damping ratio, magnitude, and distance. The SV and PSV are similar in the intermediate period range. The SV is smaller than PSV at short oscillator periods, while may be larger than PSV at longer oscillator periods. The difference between SV and PSV decreases with the increasing damping ratio, and it decreases with the increasing moment magnitude at most oscillator periods. In addition, the relationship between SV and PSV is not significantly influenced by distance.

(3) The difference between SV and PSV increases as the site varies from hard rock to soft soil at short oscillator periods, while it is nearly constant at long oscillator periods.

(4) The proposed simple *SV/PSV* model is confirmed to have good accuracy for a wide range of periods, damping ratios, magnitudes, and distances by comparing its results with the values of actual ground motion records.

## CRediT authorship contribution statement

**Zheng Liu:** Writing – original draft, Methodology, Investigation, Data curation, Conceptualization. **Yan-Gang Zhao:** Writing – review & editing, Visualization, Supervision. **Haizhong Zhang:** Writing – review & editing, Validation, Software, Methodology, Data curation, Conceptualization.

## Declaration of competing interest

The authors declare that they have no known competing financial interests or personal relationships that could have appeared to influence the work reported in this paper.

## Data availability

Data will be made available on request.

## Acknowledgments

This study was partially supported by the National Natural Science Foundation of China (Grant No. 52278135). This study used strong-motion records from K-NET and KiK-net. The authors are grateful for the financial support and earthquake data.

## References

[1] Federal Emergency Dissipation Agency (FEMA-450), NEHRP recommended provisions for seismic regulations for new buildings and other structures, Part 1: Provisions and Part 2: Commentary, Washington, D.C. FEMA P-2082-1, 2003.
[2] X.Y. Zhou, R.F. Yu, D.I. Dong, Complex mode superposition algorithm for seismic responses of non-classically damped linear MDOF system, J. Earthq. Eng. 8 (04) (2004) 597–641.
[3] R.F. Yu, X.Y. Zhou, Response spectrum analysis for non-classically damped linear system with multiple-support excitations, Bull. Earthq. Eng. 6 (2008) 261–284.
[4] Eurocode 8, Design of structures for earthquake resistance, part 1: General rules, seismic actions and rules for buildings, EN 2004-1-1, European Committee for Standardization (CEN), Brussels, Belgium, 2004.
[5] ASCE/SEI7-10, Minimum design loads for buildings and other structures, American Society of Civil Engineers, 2016.
[6] F. Sadek, B. Mohraz, M.A. Riley, Linear static and dynamic procedures for structures with velocity-dependent dampers, J. Struct. Eng. 126 (8) (2000) 887–895.
[7] J. Song, Y.L. Chu, Z. Liang, G.C. Lee, Estimation of peak relative velocity and peak absolute acceleration of linear SDOF systems, Earthq. Eng. Eng. Vib. 6 (2) (2007) 1–10.
[8] V.K. Gupta, A new approximation for spectral velocity ordinates at short periods, Earthq. Eng. Struct. Dyn. 38 (7) (2009) 941–949.
[9] G.A. Papagiannopoulos, G.D. Hatzigeorgiou, D.E. Beskos, Recovery of spectral absolute acceleration and spectral relative velocity from their pseudo-spectral counterparts, Earthq. Struct. 4 (5) (2013) 489–508.
[10] R.S. Desai, S.N. Tande, Estimation of spectral velocity at long periods for application in velocity dependent seismic energy management devices, J. Struct. Eng. 44 (1) (2017) 14–22.
[11] R.S. Desai, S.N. Tande, Estimate of peak relative velocity from conventional spectral velocity for response spectrum based force evaluation in damping devices, Struct 15 (2018) 378–387.
[12] N. Samdaria, V.K. Gupta, A new model for spectral velocity ordinates at long periods, Earthq. Eng. Struct. Dyn. 47 (1) (2018) 169–194.
[13] A. Pal, V.K. Gupta, A note on spectral velocity approximation at shorter intermediate periods, Soil Dyn. Earthq. Eng. 141 (2021) 106422.
[14] M.A. Santos-Santiago, S.E. Ruiz, F. Valenzuela-Beltrán, Influence of higher modes of vibration on the seismic response of buildings with linear and nonlinear viscous dampers, J. Earthq. Eng. 26 (8) (2022) 3914–3937.
[15] Z. Liu, Y.G. Zhao, H.Z. Zhang, Pseudo-Velocity Response Spectrum to Velocity Response Spectrum Conversion Model, J. Earthq. Eng. 1–26 (2024).
[16] GB50010-2010, Code for design of concrete structures, Beijing: China Architecture and Building Press, 2016. (in Chinese).
[17] Building Standard Law, Notification no. 631 of the ministry of land, infrastructure, transport and tourism, Earthquake-Resistant Structural Calculation Based on Energy Balance, Tokyo, Japan, 2005.
[18] H.Z. Zhang, Y.G. Zhao, Effects of magnitude and distance on spectral and pseudospectral acceleration proximities for high damping ratio, Bull. Earthq. Eng. 20 (8) (2022) 3715–3737.
[19] B.J. Hang, H.Z. Zhang, Y.G. Zhao, Effects of magnitude, epicentral distance, and site class on the relationship between spectral and pseudospectral acceleration, Earthq. Eng. Eng. Dyn. 42 (2022) 219–228, in Chinese.
[20] D.M. Boore, Simulation of ground motion using the stochastic method, Pure Appl. Geophys. 160 (2003) 635–676.
[21] D.E. Cartwright, M.S. Longuet-Higgins, The statistical distribution of the maxima of a random function. Proceedings of the Royal Society of London Series A, Mathematical and Physical Sciences, 237 (1209) (1956) 212–232.
[22] A.G. Davenport, Note on the distribution of the largest value of a random function with application to gust loading, Proc. Inst. Civ. Eng. 28 (2) (1964) 187–196.
[23] E.H. Vanmarcke, On the Distribution of the First-Passage Time for Normal Stationary Random Processes, J. Appl. Mech. 42 (1) (1975) 2130–2135.

[24] E.M. Rathje, M.C. Ozbey, Site-specific validation of random vibration theory-based seismic site response analysis, J. Geotech. Geoenviron Eng. 132 (7) (2006) 911–922.
[25] X. Wang, E.M. Rathje, Influence of peak factors on site amplification from random vibration theory based site-response analysis, Bull. Seismol. Soc. Am. 106 (4) (2016) 1733–1746.
[26] D.M. Boore, E.M. Thompson, Revisions to some parameters used in stochastic-method simulations of ground motion, Bull. Seismol. Soc. Am. 105 (2A) (2015) 1029–1041.
[27] H.Z. Zhang, Y.G. Zhao, Damping modification factor based on random vibration theory using a source-based ground-motion model, Soil Dyn. Earthq. Eng. 136 (2020) 106225.
[28] D.M. Boore, SMSIM: Fortran programs for simulating ground motions from earthquakes: version 2.3, A Revision of OFR 96–80-A, U.S, Geol Surv Dep Interior (2005).
[29] D.M. Boore, Stochastic simulation of high-frequency ground motions based on seismological models of the radiated spectra, Bull. Seismol. Soc. Am. 73 (6A) (1983) 1865–1894.
[30] N.C. Nigam, P.C. Jennings, Calculation of response spectra from strong-motion earthquake records, Bull. Seismol. Soc. Am. 59 (2) (1969) 909–922.
[31] Y. Okada, K. Kasahara, S. Hori, K. Obara, S. Sekiguchi, H. Fujiwara, A. Yamamoto, Recent progress of seismic observation networks in Japan—Hi-net, F-net, K-NET and KiK-net—, Earth. Planets Space. 56 (2004) xv–xxviii.
[32] S. Aoi, T. Kunugi, H. Nakamura, H. Fujiwara, Deployment of new strong motion seismographs of K-NET and KiK-net, Earthquake Data in Engineering Seismology: Predictive Models, Data Management and Networks. (2011) 167–186.
[33] H.Z. Zhang, Y.G. Zhao, Damping Modification Factor of Acceleration Response Spectrum Considering Seismological Effects, J. Earthq. Eng. 26 (2022) 8359–8382.
[34] H.Z. Zhang, J. Deng, Y.G. Zhao, Damping modification factor of pseudo-acceleration spectrum considering influences of magnitude, distance and site conditions, Earthq. Struct. 25 (5) (2023) 325.
[35] E. Kalkan, An automatic P-phase arrival-time picker, Bull. Seismol. Soc. Am. 106 (3) (2016) 971–986.
[36] M. Bahrampouri, A. Rodriguez-Marek, S. Shahi, H. Dawood, An updated database for ground motion parameters for KiK-net records, Earthq. Spectra. 37 (1) (2021) 505–522.